ECCOMAS Congress 2016
VII European Congress on Computational Methods in Applied Sciences and Engineering
M. Papadrakakis, V. Papadopoulos, G. Stefanou, V. Plevris (eds.)
Crete Island, Greece, 5–10 June 2016

HOMOGENIZATION METHOD FOR DESIGNING NOVEL ARCHITECTURED CELLULAR MATERIALS

Zheng-Dong Ma[1]

[1] The University of Michigan
Ann Arbor, Michigan, USA
e-mail: mazd@umich.edu

Keywords: Homogenization Method, Discrete Homogenization Method, Cellular Materials, Architectured Materials, Coordinate Reduction, Computational Method.

Abstract. *Two types of novel architectured cellular materials have been developed [1,2]. To estimate the effective material properties and to optimally design such materials, a suitable homogenization method was needed. An existing asymptotic homogenization process has provided an effective means for the multiscale modeling of continuum solids; however, that method was not easily adapted to the aforementioned materials, which are naturally discrete systems. First, we developed a strain-based homogenization method equivalent to the existing asymptotic homogenization method, but it was developed based on an engineering approach rather than on a mathematical approach such as the one used in asymptotic homogenization. The new approach separates the strain field into a homogenized strain field and a strain variation field in the local cellular domain superposed on the homogenized strain field. The Principle of Virtual Displacements for the relationship between the strain variation field and the homogenized strain field is then used to condense the strain variation field onto the homogenized strain field, and the homogenization process becomes a coordinate reduction process comparable to the Guyan Reduction used in structural dynamics analyses. The characteristic modes and the stress recovery process are also discussed. The new method is then extended to a stress-based homogenization process based on the Principle of Virtual Forces, and it is further applied to address the discrete systems of the aforementioned architectured cellular materials.*

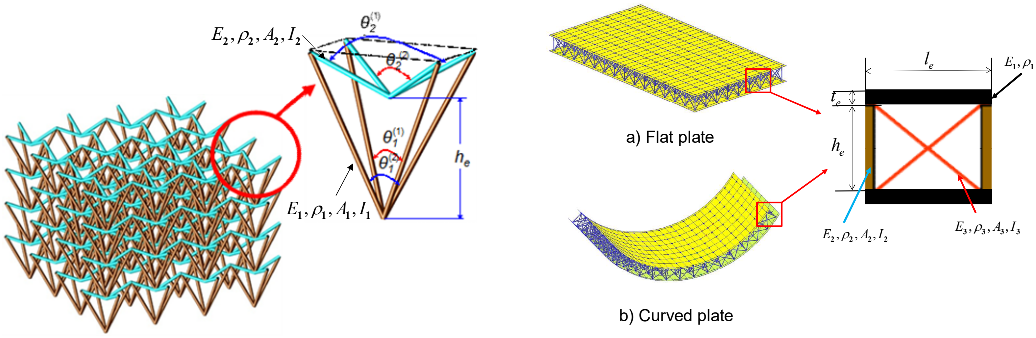

3D NPR material [1]

b) BTR material [2]

Figure 1: Novel architectured cellular materials.

1 INTRODUCTION

Multiscale modeling and homogenization have become rich areas of research. Fruitful results have been published with a wide range of applications, as listed in recent literature review papers [3-5]. Homogenization, especially asymptotic homogenization [6-8], provides a powerful mathematical tool for bridging different scale modeling problem, and solving micro-macro, local-global, nano-macro, etc., multiscale modeling problems. The applicable areas include so-called heterogeneous materials, cellular materials, granular materials, fiber-reinforced polymers, etc. The homogenization method has also been utilized in topology optimization processes [9-11].

Two types of useful architectured cellular materials have been developed in the literature [1,2]. One type is three-dimensional Negative Poisson's Ratio (NPR) materials [1] (shown in Fig. 1a), and the other is so-called Biomimetic Tendon-Reinforced (BTR) materials [2] (shown in Fig. 1b). Both are originally obtained through the topology optimization process developed in [9]. These new materials are similar to traditional lattice materials, but they can be made of multiple raw materials and cannot be referred to as "micro" because of their relatively larger sizes. To estimate the effective material properties and to optimally design such materials, a suitable homogenization method was needed.

The advantages in the mathematical process of asymptotic homogenization should be appreciated; however, they are often overlooked in favor of the "mechanics logics" inside the homogenization modeling process. Existing asymptotic homogenization methods have provided effective means for the multiscale modeling of continuum solids; however, there is a need for extending them to more general applications such as handling the discrete systems discussed in this paper.

This paper provides a view of the existing homogenization process that is based on engineering and mechanics rather than on mathematics. Furthermore, most discoveries in this paper actually exist elsewhere in various previous publications [12-16]; however, it is useful to provide a more systematic explanation for mechanics-based homogenization. Another important point is that theoretically the mathematical asymptotic homogenization process requires the micro-cell to be small or infinitely small to assume convergence of the process, but this is not necessary for mechanics-based homogenization. In fact, mechanics-based homogenization can be considered a coordinate reduction process like the *Guyan Reduction* [17], which is widely used in solving structural dynamics problems. Therefore, relatively larger size cells can be treated in various applications, including in architectured cellular materials.

First, continuum solids are considered, and a mechanics-based homogenization process is developed based on the *Principle of Virtual Displacements*. Although the resultant formulations for the homogenized material stiffness matrix are the same as those obtained from the asymptotic homogenization method, mechanics-based homogenization provides a better understanding in terms of the mechanics behind the homogenization process. The new approach separates the strain field into a homogenized strain field along with a strain variation field in the local cellular domain superposed on the homogenized strain field. The *Principle of Virtual Displacements* describing the relationship between the strain variation field and the homogenized strain field is then used to condense the strain variation field to the homogenized strain field. Hence, the homogenization process is treated as a coordinate reduction process like the *Guyan Reduction*.

New formulas are also obtained to calculate the effective mass density and body forces with improved approximations, which can be further extended to consider other body forces such as thermal and magnetic forces. The characteristic stain modes and corresponding characteristic displacement modes are discussed. A recovery process is further considered for recovering the local strain and stress in the cellular domain after the global analysis.

The new method can have two variants: one is strain-based homogenization, and the other is stress-based homogenization. The stress-based homogenization process is obtained based on the *Principle of Virtual Forces*. Similar to strain-based homogenization, strain-based homogenization separates the stress field into a homogenized stress field and a stress variation field superposed on the homogenized stress field. The principle of virtual forces is then used to condense the stress variation field into the homogenized stress field. The stress-based homogenization process can be extended easily to address discrete systems. The new method is then utilized to obtain the effective material properties of the architectured cellular materials discussed in this paper.

2 THE ASYMPTOTIC HOMOGENIZATION METHOD

An asymptotic homogenization method [3-5] for an elastostatic continuum is derived using the mathematical approach described below. First, supposing that the structure in a domain Ω_ε has a Y-periodic microstructure, the state equation can be written as:

$$\int_{\Omega_\varepsilon} E^{\varepsilon}_{ijkl} \frac{\partial u^{\varepsilon}_i}{\partial y_j} \frac{\partial v_k}{\partial y_l} d\Omega + \int_{\Omega_\varepsilon} f_i v_i d\Omega + \int_{\Gamma_t} t_i v_i d\Gamma = 0 \quad \text{for } \forall v \in V . \tag{1}$$

The periodic microstructure is assumed to be near to an arbitrary point x of a given linearly elastic structure. The periodicity is represented by a parameter ε, which is very small, and the elastic tensor is given in the form of

$$E^{\varepsilon}_{ijkl} = E_{ijkl}\left(x,\ \frac{x}{\varepsilon} \right), \tag{2}$$

where $y \to E_{ijkl}(x, y)$ is Y-periodic, x is the macroscopic variation of the material parameters, and $y = x/\varepsilon$ gives the microscopic, periodic variations. Now, supposing that the structure is subjected to a macroscopic body force and a macroscopic surface traction, the resulting displacement field $u^{\varepsilon}(x)$ can then be expanded as

$$u^{\varepsilon}(x) = u_0(x) + \varepsilon u_1\left(x,\ \frac{x}{\varepsilon} \right) + \varepsilon^2 u_2\left(x,\ \frac{x}{\varepsilon} \right) + \cdots, \tag{3}$$

where the leading term $u_0(x)$ is a macroscopic deformation field that is independent of the microscopic variable. Substituting Eqs. (2) and (3) into Eq. (1) and comparing the terms in the same order of ε, one can obtain the effective rigidity tensor

$$E^{H}_{ijkl}(x) = \frac{1}{|Y|} \int_Y \left[E_{ijkl}(x, y) - E_{ijpq}(x, y) \frac{\partial \chi^{kl}_p}{\partial y_q} \right] dy . \tag{4}$$

Here, χ^{kl} is a microscopic displacement field that is given as the Y-periodic solution of the cell problem in the weak form

$$\int_Y E_{ijpq} \frac{\partial \chi^{kl}_p}{\partial y_q} \frac{\partial v_i(y)}{\partial y_j} dy = \int_Y E_{ijkl} \frac{\partial v_i(y)}{\partial y_j} dy . \tag{5}$$

The homogenized equation of Eq. (1) becomes

$$\int_{\Omega} E^{H}_{ijkl} \frac{\partial u_i}{\partial y_j} \frac{\partial v_k}{\partial y_l} d\Omega + \int_{\Omega} f^{H}_i v_i d\Omega + \int_{\Gamma_t} t_i v_i d\Gamma = 0 \quad \text{for } \forall v \in V , \tag{6}$$

where f_i^H is an average of the force f_i on the cellular domain.

$$f_i^H = \frac{1}{|Y|}\int_Y f_i \, dy \tag{7}$$

Note that the above approach is obtained based on the assumption of infinitely small cellular cells; however, it does not explain why, in many cases, one cannot obtain better results by considering higher order terms of ε, which indicates that the Taylor expansion in Eq. (3) may not generally converge. The approach also has a theoretical limitation in the extension to larger cells. It lacks explicit instructions for how to determine the boundary conditions in a micro-cell analysis, with the exception of mentioning the use of the periodic boundary conditions. In fact, the periodic boundary conditions may not be able to remove the rigid body motion of the micro-cell, and different boundary conditions may be required to solve different subcases in the homogenization process, which will be discussed in Sec. 4.2.

3 HOMOGENIZATION AS A COORDINATE REDUCTION PROCESS

3.1 Problem Definition

The elastostatics problem in Eq. (1) is converted into a form of Principle of Virtual Displacements and extended to an elastic-dynamics problem. Ω_ε ($\Omega_\varepsilon \subset R^3$) is assumed to be the structural domain with a cellular structure that is in periodic or other forms, as long as the proper connections among the adjacent cells can be defined; Γ_t is the traction boundary of Ω_ε. The equilibrium of these types of cellular materials can be formulated by the *Principle of Virtual Displacements*:

$$\int_{\Omega_\varepsilon} \delta\boldsymbol{\varepsilon}^T \mathbf{D}^\varepsilon \boldsymbol{\varepsilon} d\Omega + \int_{\Omega_\varepsilon} \delta\mathbf{u}^T \rho^\varepsilon \ddot{\mathbf{u}} d\Omega = \int_{\Omega_\varepsilon} \delta\mathbf{u}^T \mathbf{f}^\varepsilon d\Omega + \int_{\Gamma_t} \delta\mathbf{u}^T \mathbf{t} d\Gamma_t \, , \tag{8}$$

where $\boldsymbol{\varepsilon}$ denotes the *engineering strain* vector ($\boldsymbol{\varepsilon}^T = \left\{\varepsilon_x, \varepsilon_y, \varepsilon_z, \gamma_{yz}, \gamma_{zx}, \gamma_{xy}\right\}^T$), **u** denotes the displacement vector, $\ddot{\mathbf{u}} = \dfrac{\partial^2 \mathbf{u}}{\partial t^2}$ denotes the acceleration vector, $\mathbf{f}^\varepsilon$ denotes the body force vector, and **t** is the boundary traction vector; $\delta\boldsymbol{\varepsilon}$ denotes the virtual stain vector, $\delta\mathbf{u}$ denotes the virtual displacement vector, $V = \left\{\delta\mathbf{u} \in \mathrm{H}^1(\Omega_\varepsilon) \mid \delta\mathbf{u}|_{\Gamma_d} = 0\right\}$ denotes the space of kinematically admissible displacement fields, and Γ_d is the displacement boundary. $\mathrm{H}^1(\Omega_s)$ is the Sobolev space in which the strain energy of the structure is finite. $\mathbf{D}^\varepsilon$ denotes the elasticity matrix before the homogenization, and ρ^ε is the density before the homogenization.

For simplicity, in the following, we assume a three-dimensional solids problem, even though the formulation obtained can be applied to two-dimensional solids problems and problems such as beams, plates, or shells. We also assume a linear elasticity problem with a constitute law $\boldsymbol{\sigma} = \mathbf{D}\boldsymbol{\varepsilon}$, where $\boldsymbol{\sigma}$ is a Cauchy stress vector ($\boldsymbol{\sigma}^T = \left\{\sigma_x, \sigma_y, \sigma_z, \tau_{yz}, \tau_{zx}, \tau_{xy}\right\}^T$), and $\mathbf{D} = \left[D_{ij}\right]_{6\times 6}$ is the material stiffness matrix, even though the formulation obtained can be extended easily to nonlinear problems.

Note, the *Principle of Virtual Displacements* requires the following continuity conditions to be satisfied:

$$\boldsymbol{\varepsilon} = \mathbf{E}(\nabla)\mathbf{u}, \quad \delta\boldsymbol{\varepsilon} = \mathbf{E}(\nabla)\delta\mathbf{u} \tag{9}$$

where

$$\mathbf{E}(\nabla)=\begin{bmatrix} \frac{\partial}{\partial x} & 0 & 0 & 0 & \frac{\partial}{\partial z} & \frac{\partial}{\partial y} \\ 0 & \frac{\partial}{\partial y} & 0 & \frac{\partial}{\partial z} & 0 & \frac{\partial}{\partial x} \\ 0 & 0 & \frac{\partial}{\partial z} & \frac{\partial}{\partial y} & \frac{\partial}{\partial x} & 0 \end{bmatrix}^{\mathbf{T}} \tag{10}$$

3.2 Homogenized Process as a Coordinate Reduction

The asymptotic homogenization method described in Sec. 2 is derived from a mathematical treatment. Now, we employ an approach based on an engineering approach and the mechanics of the problem. We consider mechanics-based homogenization as a coordinate reduction process that is analogous to the *Guyan Reduction* described in Appendix A.

Instead of separating the nodal coordinates into internal coordinates and boundary coordinates as in the *Guyan Reduction*, we separate the strain field $\boldsymbol{\varepsilon}$ into a homogenized strain field $\boldsymbol{\varepsilon}_h$ that is constant over the cellular domain and continuous over the homogenized structural domain, and a strain variation field $\boldsymbol{\varepsilon}_v=\boldsymbol{\varepsilon}_v(y)$ ($y\in Y$) superposed on $\boldsymbol{\varepsilon}_h$, which is defined in cellular Y domain and varies in Y, to obtain

$$\boldsymbol{\varepsilon}=\boldsymbol{\varepsilon}_h+\boldsymbol{\varepsilon}_v . \tag{11}$$

The displacement fields corresponding to $\boldsymbol{\varepsilon}_h$ and $\boldsymbol{\varepsilon}_v$ are denoted as $\mathbf{u}_h$ and $\mathbf{u}_v$, and we get

$$\mathbf{u}=\mathbf{u}_h+\mathbf{u}_v , \tag{12}$$

as well as the following relationships:

$$\boldsymbol{\varepsilon}_h=\mathbf{E}(\nabla)\mathbf{u}_h \quad (in\ \Omega) \quad \textbf{and} \quad \boldsymbol{\varepsilon}_v=\mathbf{E}(\nabla)\mathbf{u}_v \quad (in\ Y) . \tag{13}$$

Substituting Eq. (11) into Eq. (8) produces

$$\int_{\Omega_\varepsilon}\left(\delta\boldsymbol{\varepsilon}_h+\delta\boldsymbol{\varepsilon}_v\right)^T\mathbf{D}^\varepsilon\left(\boldsymbol{\varepsilon}_h+\boldsymbol{\varepsilon}_v\right)d\Omega+\int_{\Omega_\varepsilon}\delta\mathbf{u}^T\rho^\varepsilon\ddot{\mathbf{u}}d\Omega=\int_{\Omega_\varepsilon}\delta\mathbf{u}^T\mathbf{f}^\varepsilon d\Omega+\int_{\Gamma_t}\delta\mathbf{u}^T\mathbf{t}d\Gamma_t . \tag{14}$$

Equation (14) can be separated as

$$\begin{cases}\displaystyle\int_{\Omega_\varepsilon}\delta\boldsymbol{\varepsilon}_h^T\mathbf{D}^\varepsilon\left(\boldsymbol{\varepsilon}_h+\boldsymbol{\varepsilon}_v\right)d\Omega+\int_{\Omega_\varepsilon}\delta\mathbf{u}^T\rho^\varepsilon\ddot{\mathbf{u}}d\Omega=\int_{\Omega_\varepsilon}\delta\mathbf{u}^T\mathbf{f}^\varepsilon d\Omega+\int_{\Gamma_t}\delta\mathbf{u}^T\mathbf{t}d\Gamma_t \\ \displaystyle\int_Y\delta\boldsymbol{\varepsilon}_v^T\mathbf{D}^\varepsilon\left(\boldsymbol{\varepsilon}_h+\boldsymbol{\varepsilon}_v\right)dy=0 \qquad (\forall Y\subset\Omega_\varepsilon)\end{cases} . \tag{15}$$

Notably, if both equations in Eq. (15) are satisfied while satisfying the continuity conditions in Eq. (13) and the connectivity among adjacent cells, then the original equation, Eq. (14) (i.e., Eq. (8)), will be satisfied. Here, theoretically, we do not have to assume that the cellular Y domain is small.

To solve the second equation in Eq. (15), we represent the strain variation $\boldsymbol{\varepsilon}_v=\boldsymbol{\varepsilon}_v(y)$ with a mode superposition technique; whereas, in Eq. (16), $\boldsymbol{\varphi}(y)$ is a matrix constructed of *d* modes (*d*=6 for the three-dimensional solids, *d*=3 for the two-dimensional solids, and *d* can be other numbers for, e.g., beams, plates, and shells problems) with $\boldsymbol{\varepsilon}_h$ as the modal coordinates, namely

$$\boldsymbol{\varepsilon}_v(y)=\boldsymbol{\varphi}(y)\boldsymbol{\varepsilon}_h \qquad (y\in Y). \tag{16}$$

Note, Eq. (16) is an equivalent transformation; therefore, there is no error induced as long as the modes in $\boldsymbol{\varphi}$ are linearly independent. Substituting Eq. (16) into the second row equation in Eq. (15) results in

$$\left[\int_Y \delta\boldsymbol{\varepsilon}_v^T\mathbf{D}^{\varepsilon}\left(\mathbf{I}+\boldsymbol{\varphi}\right)dy\right]\boldsymbol{\varepsilon}_h=0 \tag{17}$$

or

$$\int_Y \delta\boldsymbol{\varepsilon}_v^T\mathbf{D}^{\varepsilon}\left(\mathbf{I}+\boldsymbol{\varphi}\right)dy=0\,. \tag{18}$$

Solving Eq. (18) with the continuity conditions in Eq. (13) and the properly defined boundary conditions (periodic boundary conditions for now), we obtain $\boldsymbol{\varphi}(y)$ ($y\in Y$), and $\boldsymbol{\varepsilon}_v$ now becomes a function of $\boldsymbol{\varepsilon}_h$. We now assume that the displacement field corresponding to $\boldsymbol{\varepsilon}_v$ can be obtained as

$$\mathbf{u}_v=\boldsymbol{\theta}(\mathbf{y})\mathbf{u}_h \qquad (y\in Y), \tag{19}$$

where $\boldsymbol{\theta}(\mathbf{y})$ satisfies

$$\boldsymbol{\varphi}(y)=\mathbf{E}(\nabla)\boldsymbol{\theta}(y) \qquad (y\in Y). \tag{20}$$

Then, substituting Eqs. (16) and (19) into the first row equation in Eq. (15) results in

$$\int_\Omega \delta\boldsymbol{\varepsilon}_h^T\mathbf{D}^H\boldsymbol{\varepsilon}_h d\Omega+\int_\Omega \delta\mathbf{u}_h^T\rho^H\ddot{\mathbf{u}}_h d\Omega=\int_\Omega \delta\mathbf{u}_h^T\mathbf{f}^H d\Omega+\int_{\Gamma_t}\delta\mathbf{u}_h^T\mathbf{t}^H d\Gamma_t \tag{21}$$

where, Ω stands for the homogenized domain of Ω_ε, and

$$\mathbf{D}^H=\frac{1}{|Y|}\int_Y \mathbf{D}^{\varepsilon}(\mathbf{I}+\boldsymbol{\varphi})dy \tag{22}$$

$$\boldsymbol{\rho}^H=\frac{1}{|Y|}\int_Y \left(\mathbf{I}+\boldsymbol{\theta}(\mathbf{y})\right)^T\rho^{\varepsilon}\left(\mathbf{I}+\boldsymbol{\theta}(\mathbf{y})\right)dy \tag{23}$$

$$\mathbf{f}^H=\frac{1}{|Y|}\int_Y \left(\mathbf{I}+\boldsymbol{\theta}(\mathbf{y})\right)^T\mathbf{f}_v^{\varepsilon}dy \tag{24}$$

$$\mathbf{t}^H=\frac{1}{|L|}\int_{\Gamma_{tY}} \left(\mathbf{I}+\boldsymbol{\theta}(\mathbf{y})\right)^T\mathbf{t}ds \tag{25}$$

where, $\Gamma_{tY}=\Gamma_t\bigcap Y$.

Notably, the homogenized material stiffness matrix in Eq. (22) is exactly the same as in Eq. (4) obtained from the asymptotic homogenization method; however, the effective mass density in Eq. (23), the effective internal force in Eq. (24), and the effective traction in Eq. (25) are different from the traditional asymptotic homogenization process, which may provide better approximations for these quantities.

3.3 Solution using a Finite Element Method

By following a standard finite element approach and assuming an assembly of nodal displacement vectors, $\boldsymbol{\chi}=\left[\boldsymbol{\chi}^{(1)},\boldsymbol{\chi}^{(2)},...,\boldsymbol{\chi}^{(d)}\right]$ and a shape function $\mathbf{N}=\mathbf{N}(y)$ in Y, $\boldsymbol{\theta}(y)$ in Eq. (19) can be represented as

$$\boldsymbol{\theta}=\mathbf{N}(y)\boldsymbol{\chi}, \tag{26}$$

and we can have

$$\boldsymbol{\varphi}=\mathbf{B}_Y\boldsymbol{\chi} \quad \text{and} \quad \delta\boldsymbol{\varepsilon}_1=\mathbf{B}_Y\delta\boldsymbol{\xi}, \tag{27}$$

where

$$\mathbf{B}_Y=\mathbf{E}\left(\nabla\right)\mathbf{N}(y). \tag{28}$$

Substituting Eq. (27) into Eq. (18) gives

$$\int_Y \delta\boldsymbol{\xi}^T\left(\mathbf{B}_Y^T\mathbf{D}^\varepsilon\mathbf{B}_Y\right)\boldsymbol{\chi}dy+\int_Y \delta\boldsymbol{\xi}^T\mathbf{B}_Y^T\mathbf{D}^\varepsilon dy=0 \ . \tag{29}$$

Equation (29) results in the following finite element equations:

$$\mathbf{K}_Y\boldsymbol{\chi}^{(i)}=\mathbf{F}_Y^{(i)} \ \left(i=1,2,\cdots,d\right), \tag{30}$$

where

$$\mathbf{K}_Y=\int_Y\left(\mathbf{B}_Y^T\mathbf{D}^\varepsilon\mathbf{B}_Y\right)dy, \tag{31}$$

and $\mathbf{F}_Y^{(i)}$ is the i-th column in $\mathbf{F}_Y$ and

$$\mathbf{F}_Y=-\int_Y\mathbf{B}_Y^T\mathbf{D}^\varepsilon dy. \tag{32}$$

Solving Eq. (30) for $\boldsymbol{\chi}=\left[\boldsymbol{\chi}^{(1)},\boldsymbol{\chi}^{(2)},...,\boldsymbol{\chi}^{(d)}\right]$ gives

$$\boldsymbol{\chi}=\mathbf{K}_Y^{-1}\mathbf{F}_Y=-\left(\int_Y\mathbf{B}_Y^T\mathbf{D}^\varepsilon\mathbf{B}_Y dy\right)^{-1}\left(\int_Y\mathbf{B}_Y^T\mathbf{D}^\varepsilon dy\right), \tag{33}$$

and then the homogenized material stiffness matrix can be obtained as

$$\mathbf{D}^H=\frac{1}{|Y|}\int_Y\mathbf{D}^\varepsilon\left(\mathbf{I}+\mathbf{B}_Y\boldsymbol{\chi}\right)dy. \tag{34}$$

Note, it is interesting to compare Eq. (33) to Eq. (A-5) in the *Guyan Reduction* to see the similarities, as well as the similarity of the homogenization process with the *Guyan Reduction*.

3.4 Characteristic Strain Modes and Deformation Modes

Notably, $\boldsymbol{\varphi}$ in Eq. (16) is a matrix constructed of d vectors (e.g., d=6 for three-dimensional solids), namely $\boldsymbol{\varphi}=\left[\boldsymbol{\varphi}^{(1)},\boldsymbol{\varphi}^{(2)},\cdots,\boldsymbol{\varphi}^{(d)}\right]$, where each $\boldsymbol{\varphi}^{(i)}$ is labeled a *characteristic strain mode* of the cellular structure corresponding to a forced unique strain field applied over the cellular Y domain, where $i=1,\ 2,\ \cdots,\ d$. In fact, Eq. (16) can be rewritten as

$$\boldsymbol{\varepsilon}_v=\sum_{i=1}^{d}\boldsymbol{\varphi}^{(i)}\varepsilon_h^{(i)}, \tag{35}$$

where $\varepsilon_h^{(1)}=\varepsilon_x$, $\varepsilon_h^{(2)}=\varepsilon_y$, $\cdots$, $\varepsilon_h^{(d)}=\gamma_{xy}$, and $\boldsymbol{\varepsilon}_h$ can be rewritten using a strain coordinates system, $\mathbf{e}^{(i)}\ (i=1,2,\cdots,d)$, as

$$\boldsymbol{\varepsilon}_h=\sum_{i=1}^{d}\mathbf{e}^{(i)}\varepsilon_h^{(i)}. \tag{36}$$

Here, for $d=6$,

$$\mathbf{e}^{(1)}=\begin{Bmatrix}1\\0\\0\\0\\0\\0\end{Bmatrix},\ \mathbf{e}^{(2)}=\begin{Bmatrix}0\\1\\0\\0\\0\\0\end{Bmatrix},\ \cdots,\ \mathbf{e}^{(6)}=\begin{Bmatrix}0\\0\\0\\0\\0\\1\end{Bmatrix}. \tag{37}$$

By substituting Eqs. (35) and (36) into the second row equation in Eq. (16), the equation for each *characteristic strain mode* $\boldsymbol{\varphi}^{(i)}$ can be obtained:

$$\int_Y \delta\boldsymbol{\varepsilon}_v^T\mathbf{D}^\varepsilon\boldsymbol{\varphi}^{(i)}dy+\int_Y \delta\boldsymbol{\varepsilon}_v^T\mathbf{D}^\varepsilon\mathbf{e}^{(i)}dy=0\ \ (i=1,\ 2,\ \cdots,\ d). \tag{38}$$

Equation (38) describes the physical meaning of the *characteristic strain mode* $\boldsymbol{\varphi}^{(i)}$, which is the response to an applied uniform unit strain field $\mathbf{e}^{(i)}$ in the cellular domain. As shown in the second term of Eq. (38), each uniform stain $\mathbf{e}^{(i)}$ results in a stress field, described as a pre-stress applied in the cellular domain, such that:

$$\boldsymbol{\sigma}_0^{(i)}=\mathbf{D}^\varepsilon\mathbf{e}^{(i)}\ \ \left(i=1,\ 2,\ \cdots,\ d\right). \tag{39}$$

Therefore, Eq. (38) can also be rewritten as

$$\int_Y \delta\boldsymbol{\varepsilon}_v^T\mathbf{D}^\varepsilon\boldsymbol{\varphi}^{(i)}dy+\int_Y \delta\boldsymbol{\varepsilon}_v^T\boldsymbol{\sigma}_0^{(i)}dy=0\quad (i=1,\ 2,\ \cdots,\ d). \tag{40}$$

The *characteristic deformation modes* of the cell can be obtained by solving Eq. (30) with the following loading condition:

$$\mathbf{F}_Y^{(i)}=-\int_Y \mathbf{B}_Y^T\mathbf{D}^\varepsilon\mathbf{e}^{(i)}dy\ \ \left(i=1,\ 2,\ \cdots,\ d\right). \tag{41}$$

Solving Eq. (30) with Eq. (41) for $\boldsymbol{\chi}^{(i)}$ results in

$$\boldsymbol{\chi}^{(i)} = -\left(\int_Y \mathbf{B}^T\mathbf{D}^{\varepsilon}\mathbf{B}dy\right)^{-1}\left(\int_Y \mathbf{B}^T\mathbf{D}^{\varepsilon}\mathbf{e}^{(i)}dy\right) \quad (i = 1,\ 2,\ \cdots,\ d). \tag{42}$$

As a special example, for a two-dimensional solid problem, we have $\boldsymbol{\varepsilon}^T = \{\varepsilon_x, \varepsilon_y, \gamma_{xy}\}^T$, $\mathbf{u}^T = \{u_x, u_y\}^T$, $\mathbf{f}^T = \{f_x, f_y\}^T$, $\mathbf{t}^T = \{t_x, t_y\}^T$, and $\boldsymbol{\varepsilon}_h$ can be written as

$$\boldsymbol{\varepsilon}_h = \sum_{i=1}^{3} \mathbf{e}^{(i)}\varepsilon_h^{(i)}, \tag{43}$$

where

$$\mathbf{e}^{(1)} = \begin{Bmatrix} 1 \\ 0 \\ 0 \end{Bmatrix},\ \mathbf{e}^{(2)} = \begin{Bmatrix} 0 \\ 1 \\ 0 \end{Bmatrix},\ \mathbf{e}^{(3)} = \begin{Bmatrix} 0 \\ 0 \\ 1 \end{Bmatrix}. \tag{44}$$

Figure 2 illustrates the uniform unit strain fields in Eq. (44) applied in the two-dimensional cellular domain.

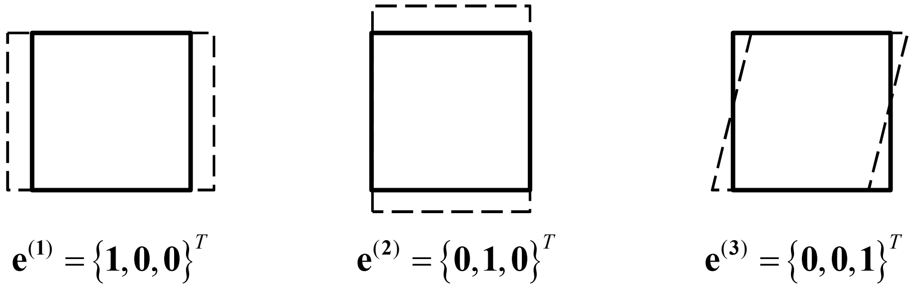

Figure 2: The unit uniform strain field $\mathbf{e}^{(i)}$ $(i = 1,2,3)$ applied in the 2-dimesional cellular domain.

Note, in Eq. (43), it is assumed that $\varepsilon_h^{(1)} = \varepsilon_x$, $\varepsilon_h^{(2)} = \varepsilon_y$, $\varepsilon_h^{(3)} = \gamma_{xy}$.

3.5 Strain and Stress Recoveries

When the global analysis is conducted and the homogenized strain $\boldsymbol{\varepsilon}_h$ is obtained, it is easy to recover the local strain in the cellular domain as

$$\boldsymbol{\varepsilon} = \boldsymbol{\varepsilon}_h + \boldsymbol{\varepsilon}_v = (\mathbf{I} + \boldsymbol{\varphi})\boldsymbol{\varepsilon}_h, \tag{45}$$

and therefore the local stress can be written as

$$\boldsymbol{\sigma} = \mathbf{D}^{\varepsilon}\boldsymbol{\varepsilon} = \mathbf{D}^{\varepsilon}(\mathbf{I} + \boldsymbol{\varphi})\boldsymbol{\varepsilon}_h = (\mathbf{I} + \boldsymbol{\varphi})\boldsymbol{\sigma}_h. \tag{46}$$

Note that these local strain and stress equations can be used to determine the failure and failure modes of cellular structures, or to predict the plastic deformation in the cellular domain. Furthermore, the failure modes can be analyzed to determine the critical loads and to improve the local architecture design of the cellular material.

4 EXTENSION TO THE STRESS-BASED HOMOGENIZATION

4.1 Continuum Systems

The elastostatics problem in Eq. (8) can also be stated using the *Principle of Virtual Forces* as

$$\int_{\Omega_\varepsilon} \delta\boldsymbol{\sigma}^T \mathbf{A}^\varepsilon \boldsymbol{\sigma} d\Omega + \int_{\Gamma_u} \delta\mathbf{p}^T \bar{\mathbf{u}} d\Gamma = 0, \tag{47}$$

where $\boldsymbol{\sigma}$ ($\boldsymbol{\sigma}^T = \left\{\sigma_x, \sigma_y, \sigma_z, \tau_{yz}, \tau_{zx}, \tau_{xy}\right\}^T$ for 3-dimensional solids) stands for the stress vector satisfying

$$\mathbf{E}(\nabla)^T \boldsymbol{\sigma} = \mathbf{f} \ \ \textbf{in}\ \Omega_\varepsilon \quad \text{and} \quad \mathbf{E}(\eta)^T \boldsymbol{\sigma} = \mathbf{t} \ \ \textbf{on}\ \Gamma_u \ , \tag{48}$$

where $\mathbf{A}^\varepsilon$ is the material flexibility matrix; in general, we obtain

$$\mathbf{A}^\varepsilon = \left[\mathbf{D}^\varepsilon\right]^{-1}. \tag{49}$$

It is also assumed that $\delta\boldsymbol{\sigma}$ satisfies

$$\mathbf{E}(\nabla)^T \delta\boldsymbol{\sigma} = 0 \ \ \textbf{in}\ \Omega_\varepsilon \quad \text{and} \quad \mathbf{E}(\nu)^T \delta\boldsymbol{\sigma} = \delta\mathbf{p} \ \ \textbf{on}\ \Gamma_u \ . \tag{50}$$

Similar to the process described in Sec. 3.2, we assume

$$\boldsymbol{\sigma} = \boldsymbol{\sigma}_h + \boldsymbol{\sigma}_v, \tag{51}$$

where $\boldsymbol{\sigma}_h$ stands for the homogenized stress field, $\boldsymbol{\sigma}_v$ is the stress variation from the homogenized stress field in the cellular domain; also, we assume

$$\mathbf{p} = \mathbf{p}_h + \mathbf{p}_v, \tag{52}$$

where $\mathbf{p}_h$ stands for the boundary force corresponding to the homogenized stress field $\boldsymbol{\sigma}_h$, $\mathbf{p}_v$ stands for the boundary force corresponding to the stress variation $\boldsymbol{\sigma}_v$. Eq. (47) can be rewritten as

$$\begin{cases} \int_{\Omega_\varepsilon} \delta\boldsymbol{\sigma}_h^T \mathbf{A}^\varepsilon \left(\boldsymbol{\sigma}_h + \boldsymbol{\sigma}_v\right) d\Omega + \int_{\Gamma_u} \delta\left(\mathbf{p}_h + \mathbf{p}_v\right)^T \bar{\mathbf{u}} d\Gamma = 0 \\ \int_Y \delta\boldsymbol{\sigma}_v^T \mathbf{A}^\varepsilon \left(\boldsymbol{\sigma}_h + \boldsymbol{\sigma}_v\right) dy = 0 \qquad \textbf{for}\ \forall Y \in \Omega \end{cases} . \tag{53}$$

Similar to the process in Sec. 3.2, we assume

$$\boldsymbol{\sigma}_h = \sum_{i=1}^{d} \mathbf{e}_1^{(i)} \sigma_h^{(i)} \ \text{and} \ \boldsymbol{\sigma}_v = \sum_{i=1}^{d} \mathbf{z}_1^{(i)} \sigma_h^{(i)}. \tag{54}$$

Substituting Eq. (54) into the second row equation in Eq. (53) results in

$$\int_Y \delta\boldsymbol{\sigma}_v^T \mathbf{A}^\varepsilon \mathbf{z}^{(i)} dy + \int_Y \delta\boldsymbol{\sigma}_v^T \mathbf{A}^\varepsilon \mathbf{e}_1^{(i)} dy = 0 \ \ (i = 1,\ 2,\ \cdots,\ d). \tag{55}$$

$\mathbf{z}_1^{(i)}$ $(i = 1, 2, \cdots, d)$ can be obtained by solving Eq. (55) with the properly defined (periodic) boundary conditions, and then the first row equation in Eq. (53) becomes

$$\int_{\Omega} \delta \boldsymbol{\sigma}_h^T \mathbf{A}^H \boldsymbol{\sigma}_h d\Omega + \int_{\Gamma_u} \delta \mathbf{p}_h^T \bar{\mathbf{u}}^H d\Gamma = 0, \tag{56}$$

where

$$\mathbf{A}^H = \frac{1}{|Y|} \int_Y \mathbf{A}^{\varepsilon} \left(\mathbf{I} + \mathbf{z}_1 \right) dy \text{ and} \tag{57}$$

$$\bar{\mathbf{u}}^H = \frac{1}{|L|} \int_{\Gamma_{uY}} \left(\mathbf{I} + \boldsymbol{\omega} \right)^T \bar{\mathbf{u}} ds, \tag{58}$$

such that

$$\mathbf{E}(\nu)^T \mathbf{z}_1 = \boldsymbol{\omega} \ \textbf{on} \ \Gamma_{uY} \ \ \textit{and} \ \ \Gamma_{uY} = \Gamma_u \cap Y. \tag{59}$$

Note, it is not necessary for the stress-based homogenization process to produce the same effective material properties as the strain-based homogenization process. In fact, based on the *Principle of Virtual Displacements* and *Principle of Virtual Forces*, the strain-based homogenization process may provide an upper boundary for the effective material properties; the stress-based homogenization process provides a lower bound for the effective material properties.

As a special example, for a two-dimensional solids problem, we have $\boldsymbol{\sigma}^T = \left\{ \sigma_x, \sigma_y, \tau_{xy} \right\}^T$, and $\boldsymbol{\sigma}_h$ becomes

$$\boldsymbol{\sigma}_h = \sum_{i=1}^{3} \mathbf{e}^{(i)} \sigma_h^{(i)}. \tag{60}$$

Figure 3 illustrates the uniform unit stress fields in Eq. (61) applied in the two-dimensional cellular domain.

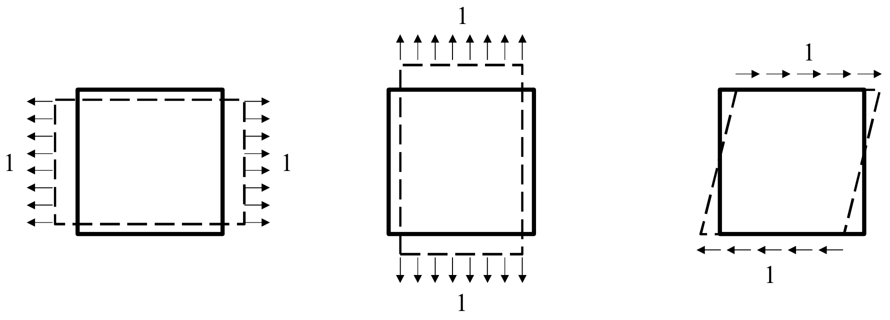

Figure 3: A unit uniform stress field $\mathbf{e}^{(i)}$ $(i = 1, 2, 3)$ applied on the 2-dimesional cellular domain.

Note that in Eq. (60), $\sigma_h^{(1)} = \sigma_x$, $\sigma_h^{(2)} = \sigma_y$, $\sigma_h^{(3)} = \tau_{xy}$ is assumed.

4.2 Extension to the Discrete Systems

With the above understanding, the extension to discrete systems can easily be performed by first, converting the applied unit stress field into concentrated forces and applying them to the proper nodes of the cellular structure; second, one must calculate the displacements at the properly selected nodes to approximate the strain in the cellular domain and use the obtained information to approximate the effective material properties. As an example, Fig. 4 uses a two-dimensional version of the NPR material shown in Fig. 1a to illustrate the loading conditions and boundary conditions for the homogenization of a 2D NPR cell structure.

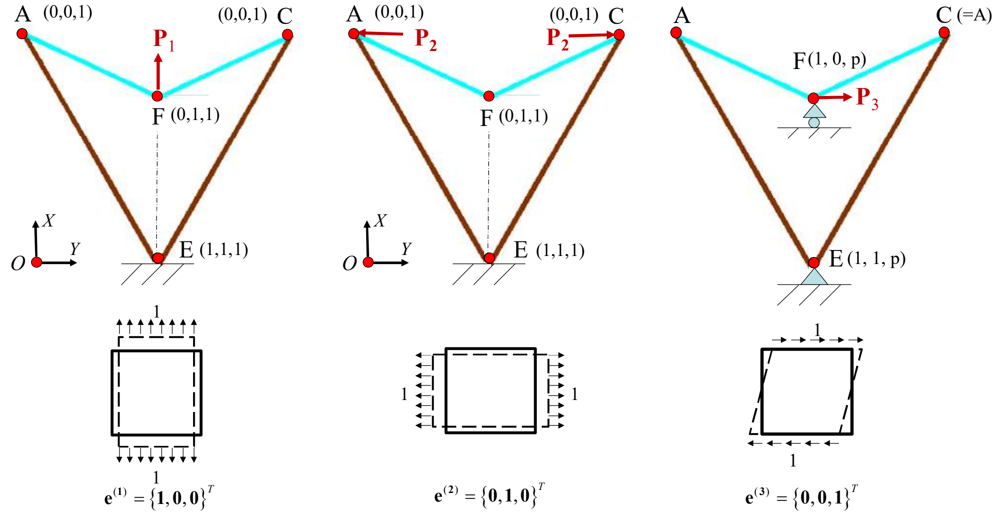

Figure 4: The loading and boundary conditions for the homogenization of a 2D NPR cell structure.

In Fig. 4, the vertical direction is set as the x-direction, and the horizontal direction is as the y-direction. As shown in Figure 4, there are three analysis cases in total corresponding to the three characteristic modes in the homogenization problem. Each loading case corresponds to a unit stress field, discussed in Sec. 4.1, with an amplitude equal to the facing area multiplied by the unit stress, which is 1. The boundary conditions are determined by the periodicity consideration as well as the symmetry of the cell structure and the connectivity to the adjacent cells.

As shown in the left figure in Fig. 4, a concentrated force P_1 is applied at Point F, which represents the tension stress on the top of the cell. Here, boundary condition E (1, 1, 1) indicates that node E is fixed along all of the directions, including the x- and y-directions as well as the deformation angle. Additionally, A (0, 0, 1) indicates that only the deformation angle is fixed at node A, and this is the same for node C.

As shown in the middle figure in Fig. 4, two concentrated forces with equal amplitudes P_2 are applied at Points A and C in opposite directions, representing the tension stress on the two sides of the cell. Here, the boundary conditions are the same as in the left figure.

The right figure in Fig. 4 illustrates a shear force applied on the cellular cell, for which C=A indicates the periodicity boundary conditions needing to be applied at nodes A and C, and F (1, 1, p) and E (1, 1, p) indicate the periodicity boundary condition for the deformation angle at nodes F and E.

Note that the boundary conditions must be considered case by case for the typical cell configuration, structural symmetry, and connectivity with the adjacent cells in addition to the periodic arrangement of the cells in the global domain.

5 EXAMPLES

5.1 Three-dimensional NPR Materials

Figure 5 illustrates the material cell model for the three-dimensional NPR materials invented in the literature [1]. NPR materials are also called auxetic, anti-rubber, and dilational materials. Since Lakes published his article in Science in 1987 [18], NPR materials have attracted increasingly more attention because of their unique behavior. Unlike conventional materials, NPR materials may shrink when compressed (expand when stretched) along the perpendicular direction. The unique features of the NPR materials include, but are not limited to, 1) stiffening under a load, 2) impact energy absorption, 3) function-graded and function-oriented design, and 4) the ability to be engineered to have other desired functionalities.

As shown in Fig. 5, the invented NPR structure comprises a pyramid-shaped unit cell having four base points, A, B, C, and D, defining the corners of a square lying in a horizontal plane. Four stuffers of equal length or different lengths extend from a respective one of the base points to a point E spaced apart from the plane. Four tendons of equal length or different lengths, but less than the lengths of the stuffers, extend from one of the base points to a point F between point E and the plane. There are, in general, five parameters that determine the cell geometry, i.e., $\theta_1^{(1)}$, $\theta_1^{(2)}$, $\theta_2^{(1)}$, $\theta_2^{(2)}$, h_e. For simplicity, in this paper, we assume $\theta_1^{(1)}=\theta_1^{(2)}=\theta_1$ and $\theta_2^{(1)}=\theta_2^{(2)}=\theta_2$, such that the geometrical parameters are reduced to three, θ_1, θ_2, h_e. The design parameters of the NPR cell also include the material properties of the stuffers and the tendons, as well as shapes of the strips and the cross-section shapes of the stuffers and tendons. In this paper, we assume that all of the strips are straight and have constant cross-sectional shapes that can be represented by E_1, A_1, I_1, ρ_1 for the stuffers and E_2, A_2, I_2, ρ_2 for the tendons. Note, in these examples, we assume both the stuffers and the tendons are made of steel.

In the three-dimensional configurations, a collection of unit cells is arranged as tiles in the same horizontal plane with the base points of each cell connected to the base points of the adjoining cells, thereby forming a horizontal layer. A collection of horizontal layers is then stacked with each point E of the cells in one horizontal layer being connected to a point F of the cells in an adjacent layer. The above facts can be used to determine the connectivity among the adjacent cells and then used to determine the boundary conditions for the cell analyses in the homogenization process.

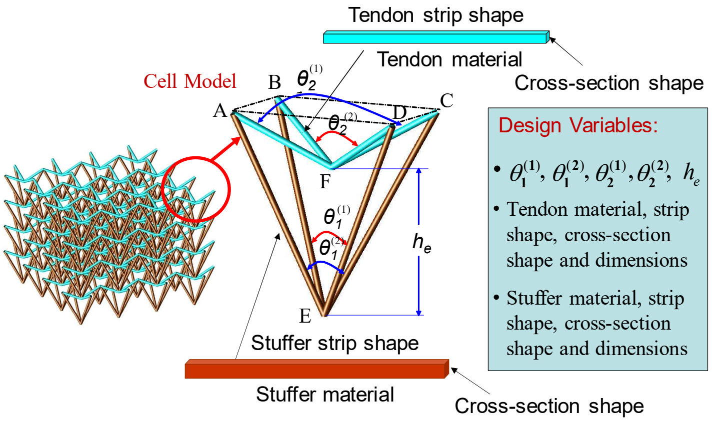

Figure 5: Design variables in a 3D NPR cell.

Figure 4 has illustrated three analytical cases with the loading and boundary conditions for the homogenization of a 2D NPR cell structure. In the following analyses, we consider the homogenization problem of a 3D NPR material shown in Fig. 5. Due to the symmetry of the cell structure, we can consider only a quarter of the cell structure, which results in a two-dimensional analysis problem, as shown in Fig. 6; meanwhile, Fig. 6 illustrates the problem setup for the first mode under a unit stress $\mathbf{e}^{(1)} = \{1,0,0,0,0,0\}^T$. Here, in Fig. 6, the concentrated force P_1 should be a quarter of the total force (unit stress multiplied by the top area of the cell) applied on the top of the cell. The boundary conditions are determined by considering the periodic conditions as well as the connectivity among the adjacent cells, as discussed in Sec. 4.2.

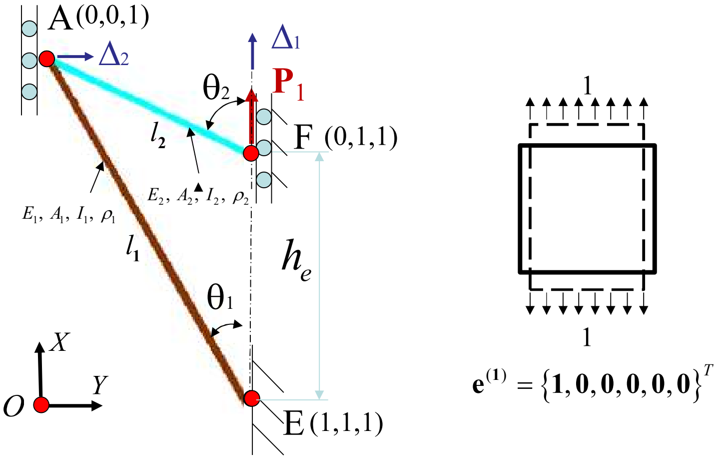

Figure 6: Analysis model for characteristic mode 1.

The analytical problem shown in Fig. 6 can be analytically solved using the assumption of the Euler–Bernoulli beam for the bending along with the tension of all of the members. As a result, we obtain the analytical solution for Δ_1 and Δ_2 as functions of P_1 as follows:

$$\begin{cases} \Delta_1 = \dfrac{\left(\mathbf{g}_{11}^1 + \mathbf{g}_{11}^2\right)\left(\mathbf{g}_{22}^1 + \mathbf{g}_{22}^2\right) - \left(\mathbf{g}_{12}^1 + \mathbf{g}_{12}^2\right)^2}{\mathbf{g}_{11}^1 + \mathbf{g}_{11}^2} P_1 \\ \Delta_2 = \dfrac{\mathbf{g}_{11}^2 \mathbf{g}_{12}^1 - \mathbf{g}_{12}^2 \mathbf{g}_{11}^1}{\mathbf{g}_{11}^1 + \mathbf{g}_{11}^2} P_1 \end{cases}, \tag{61}$$

where

$$\begin{cases} g_{11}^1 = a_1 \sin^2\theta_1 + b_1 \cos^2\theta_1 \\ g_{12}^1 = \left(a_1 - b_1\right)\sin\theta_1 \cos\theta_1 \\ g_{22}^1 = a_1 \cos^2\theta_1 + b_1 \sin^2\theta_1 \end{cases}, \quad \begin{cases} g_{11}^2 = a_2 \sin^2\theta_2 + b_2 \cos^2\theta_2 \\ g_{12}^2 = \left(a_2 - b_2\right)\sin\theta_2 \cos\theta_2 \\ g_{22}^2 = a_2 \cos^2\theta_2 + b_2 \sin^2\theta_2 \end{cases} \tag{62}$$

$$a_1 = \frac{l_1}{E_1 A_1},\ b_1 = \frac{l_1^3}{12 E_1 I_1},\ a_2 = \frac{l_2}{E_2 A_2},\ b_2 = \frac{l_2^3}{12 E_2 I_2}. \tag{63}$$

In the above formulation, there are only 3 independent design variables among θ_1, θ_2, l_1, and l_2, and the following relationship exists:

$$l_1 \sin \theta_1 = l_2 \sin \theta_2 . \tag{64}$$

The mass density can be obtained as

$$\rho^H = 4\left(\rho_1 l_1 A_1 + \rho_2 l_2 A_2\right) / V_e , \tag{65}$$

where V_e is the total volume of the cell.

Based on the above analysis, the corresponding strains along X and Y directions are obtained. Here, $\varepsilon_X = \Delta_1 / h_e$ and $\varepsilon_Y = \Delta_2 / (l_1 \sin \theta_1)$. Figure 7 illustrates the effective Young's modulus (GPa) as a function of two design variables θ_1 and θ_2. Here, the horizontal axis is θ_1, and the vertical axis is the difference angle between θ_2 and θ_1. For this typical setup, the material becomes stiffer when θ_1 becomes small and the difference between θ_2 and θ_1 becomes small; the effective Young's modulus (in black) can vary from 1 GPa to 50 GPa in the parameter range considered. Figure 7 also shows the density contour (in red) as a percentage with respect to the design variables. It is seen that the density also increases when θ_1 becomes small and the angle difference becomes small; meanwhile, from the map, the optimal designs can be obtained for the given densities. For example, a 50 GPa design can be obtained at a material density of 25% when θ_1 is approximately 8 degrees and θ_2 is 53 degrees. Figure 8 illustrates the effective Poisson's ratio (as a percentage) obtained from the analysis. It is seen that the Poisson's ratio reaches the most negative number (less than -0.6) when θ_1 is within 10-15 degrees, θ_2 is within 20-30 degrees, and the material density is near 25%. Figure 9 further illustrates the critical pressure of the cellular material, indicating that a failure analyses can also be conducted using the model developed. Notably, the analysis results depend on the other parameters used for the cell element, and studying the actual material properties is not the purpose of this paper.

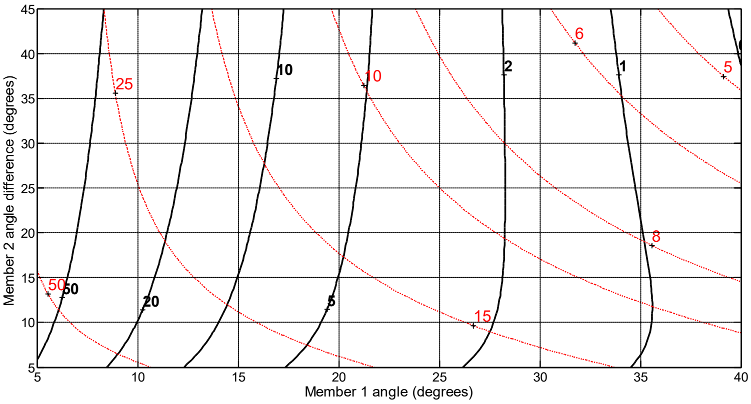

Figure 7: The effective Young's modulus (in black and GPa) for mode 1.

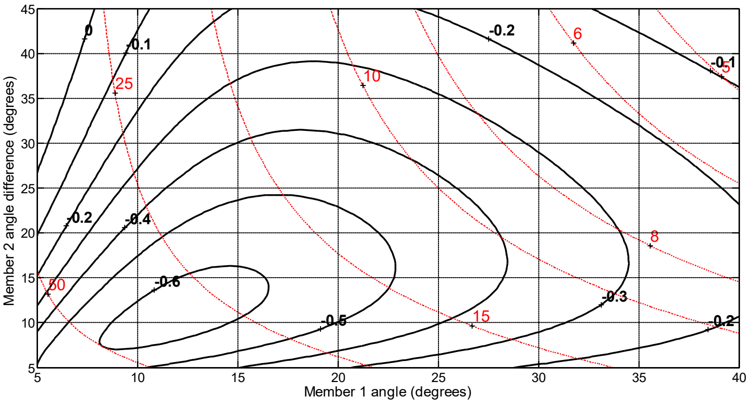

Figure 8: The effective Poisson's ratio (in black and 100%) for mode 1.

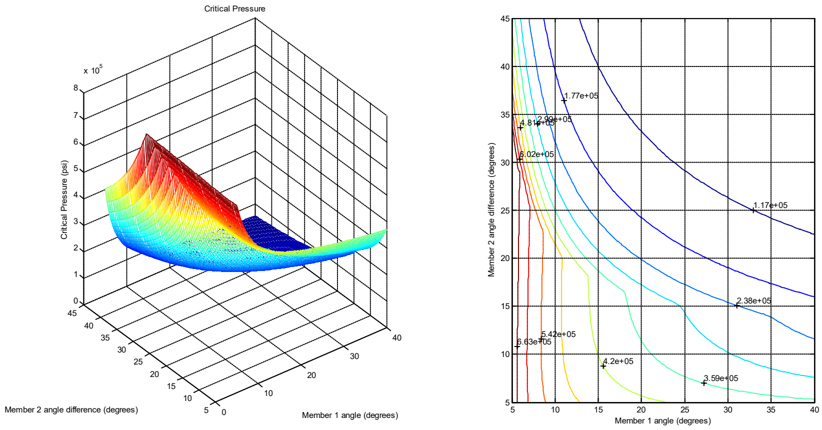

Figure 9: The critical pressure of the cellular structure for mode 1.

Figure 10 illustrates the problem setup for the second mode under a unit stress $\mathbf{e}^{(2)} = \{0,1,0,0,0,0\}^T$. Due to the symmetry of the cell structure, we can also consider only a quarter of the cell structure and a two-dimensional analysis problem, as show in Fig. 10. Here, the concentrated force P_2 should be the total force due to the unit stress applied on the side of the cell.

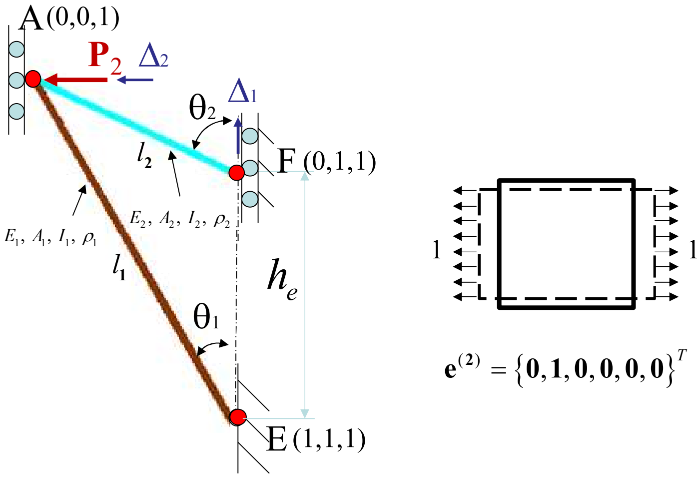

Figure 10: The analysis model for characteristic mode 2.

The analytical problem shown in Fig. 10 can be analytically solved with the same assumption as in the first case. As a result, for mode 2, we have

$$\begin{cases} \Delta_1 = \dfrac{\mathbf{g}_{11}^2\mathbf{g}_{12}^1 - \mathbf{g}_{12}^2\mathbf{g}_{11}^1}{\mathbf{g}_{11}^1 + \mathbf{g}_{11}^2} P_2 \\ \Delta_2 = \dfrac{\mathbf{g}_{11}^1\mathbf{g}_{12}^2}{\mathbf{g}_{11}^1 + \mathbf{g}_{11}^2} P_2 \end{cases} . \tag{66}$$

Figure 11 illustrates the effective Young's modulus (GPa) (in black) as a function of the two design variables θ_1 and θ_2. For this typical setup, the material becomes stiffer when θ_1 becomes larger, and the difference between θ_2 and θ_1 becomes larger; the effective Young's modulus can vary from 0.5 GPa to 20 GPa in the parameter range considered. Figure 12 illustrates the effective Poisson's ratio (100%) obtained from the analysis. The Poisson's ratio reaches the most negative number (less than -2.0) when θ_1 approaches 40 degrees and θ_2 is within 70-80 degrees. Figure 13 further illustrates the critical pressure on the side of the cellular structure indicating that side failure analyses can also be conducted using the model developed.

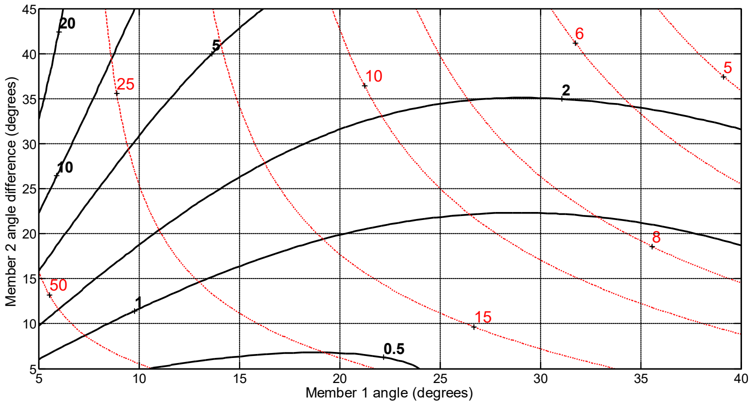

Figure 11: The effective Young's modulus (in black and GPa) for mode 2.

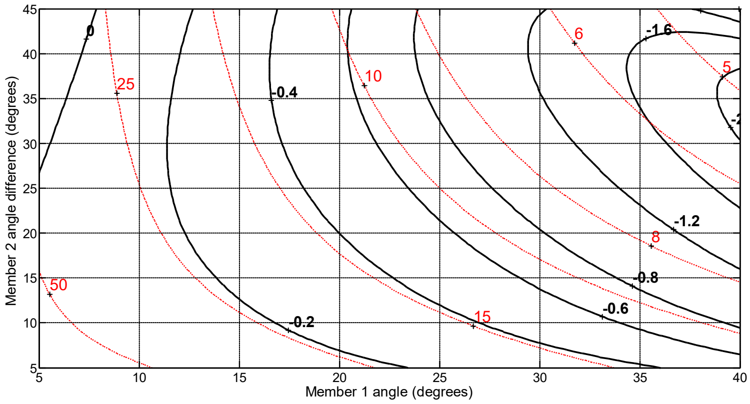

Figure 12: The effective Poisson's ratio (in black and 100%) for mode 2.

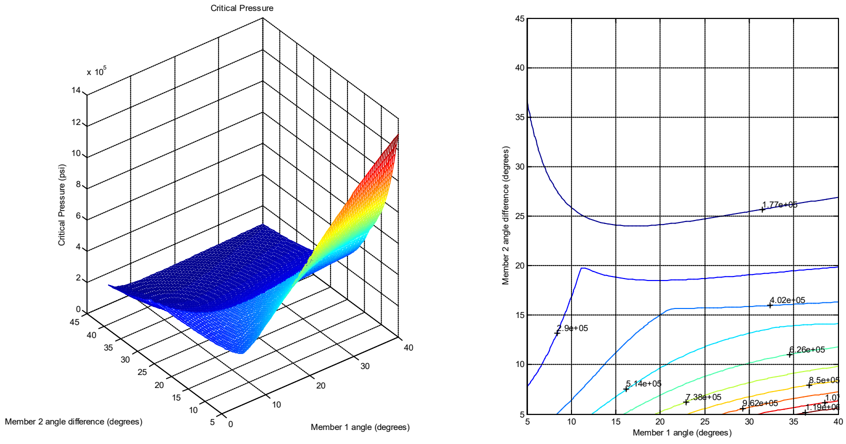

Figure 13: The critical pressure of the cellular structure for mode 2.

Note that the shear mode shown on the right in Fig. 4 and other shear modes in the three-dimensional problem can also be considered; in fact, two of the shear modes can be obtained using the analysis model shown in Fig. 4, which is omitted in this paper.

5.2 BTR Materials

Figure 14 illustrates the parameterization of the BTR materials proposed in the literature [2]. As shown in Fig. 14, BTR has three major components: 1) cover sheets on the top and bottom, which are usually made of thin composites (such as fiber-reinforced polymer) or metallic sheets; 2) stuffers, which are usually made of stiff materials such as metallic columns, ceramics, or high stiffness composites; and 3) tendons, which are usually made of high strength tension materials, such as metal wires or high strength fibers. In summary, BTR materials can be made of various raw materials depending on the applications. One of major features of the BTR materials is their lightweight characteristics and high material efficiencies, especially, for the out-of-plane bending stiffness as compared to the existing composite materials. As shown in Fig. 14, the major design parameters for the geometry of BTR materials are h_2, l_1, and t_1. Other design parameters include the material properties of sheets, stuffers, and tendons represented by E_i and ρ_i $(i=1,2,3)$, the cross-sectional area of the stuffers represented by A_2, and the cross-sectional area of the tendons, A_3.

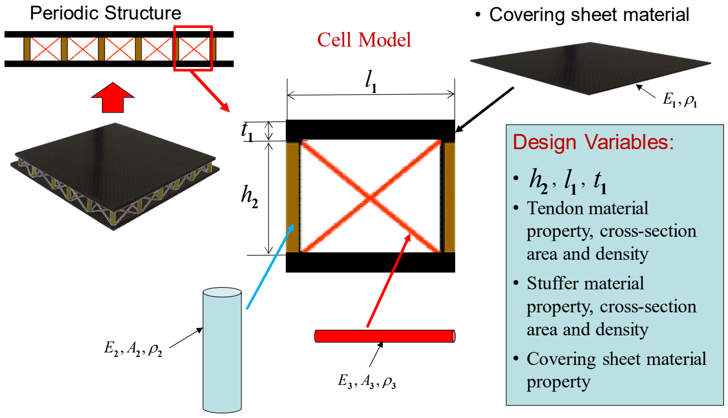

Figure 14: The design variables in a BTR cell.

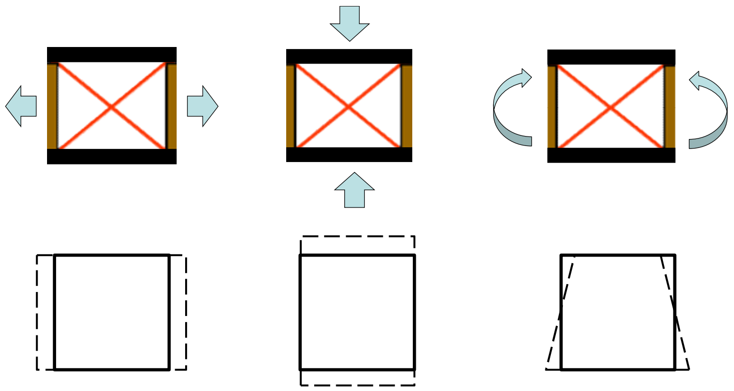

a) In-plane tension b) Out-plane compression c) Pure bending

Figure 15：The strain modes of the BTR cell.

To estimate the effective material properties of BTR materials, a strain-based homogenization process is used. Fig. 15 illustrates the three major strain modes considered in this paper. Note that the two-dimensional figures shown in Fig. 15 actually represent three-dimensional structures. Additionally, note that because a major advantage of BTR materials is the high out-of-plane bending stiffness and out-of-plane bending strength, the effective bending stiffness is considered (Fig. 15c) instead of shear modulus.

From Fig. 15a, the homogenized in-plane tension modulus $E^H_{in-plane}$ can be obtained as

$$E^H_{in-plane} = \frac{2t_1}{h_2 + 2t_1} E_1 + \frac{2 l_1^2 A_3}{(h_2 + 2t_1)\left(l_1^2 + h_2^2\right)^{\frac{3}{2}}} E_3 . \tag{67}$$

From Fig. 15b, the homogenized out-of-plane compression modulus $E^H_{out-plane}$ can be obtained as

$$E^H_{out-plane} = \frac{1}{l_1^2}\left(\frac{(h_2 + 2t_1) E_1 E_2}{h_2 E_1 + 2t_1 E_2} A_2 + \frac{4(h_2 + 2t_1) h_2^3 A_3}{l_1 \left(l_1^2 + h_2^2\right)^{\frac{3}{2}}} E_3 \right). \tag{68}$$

From Fig. 15c, the homogenized (unit) bending stiffness $(EI)^H_{bending}$ can be obtained as

$$(EI)^H_{bending} = \frac{1}{12} E_1 \left[(h_2 + 2t_1)^3 - (h_2)^3 \right]. \tag{69}$$

And the effective mass density ρ^H can be obtained as

$$\rho^H = \frac{2t_1}{h_2 + 2t_1} \rho_1 + \frac{A_2}{l_1^2} \rho_2 + \frac{4\sqrt{l_1^2 + h_2^2}\, A_3}{l_1^2 h_2} \rho_3 . \tag{70}$$

Figures 16-18 illustrate example results obtained from the above formulations for a typical design case. Here, only two design variables, the stuffer height h_2 and the sheet thickness t_1, are varied for the parametric studies. Note that all of the results in Figs. 16-18 are normalized with the initial values $t_1 = 1$ mm and $h_2 = 15$ mm.

Figure 16 shows the normalized bending stiffness with the normalized area density. The bending stiffness increases by increasing either design parameter, but an increase in the stuffer height is more effective than increasing the sheet thickness. This map is useful for selecting a proper design. For example, by selecting $t_1 = 1.5$ mm and $h_2 = 21.6$ mm, we can increase the bending stiffness 3 times while only increasing the area density by 1.4 times.

Figure 17 shows the normalized in-plane modulus with the normalized area density. The in-plane modulus is insensitive to the design changes in this case. Figure 18 further shows the normalized out-plane modulus with the normalized area density. In this case, the out-of-plane modulus decreases when the stuffer height is increased, and it is less sensitive to design changes in the sheet thickness. Note that the analysis results also depend on the other parameters used for the cell element and studying the actual material properties is not the purpose of this paper.

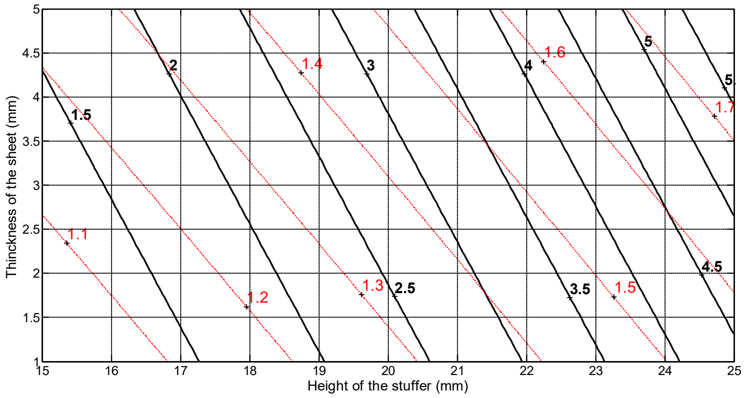

Figure 16： The normalized bending stiffness – normalized area density map.

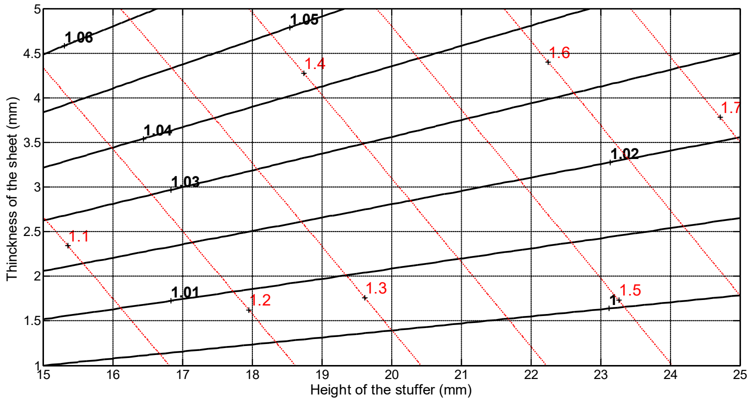

Figure 17： The normalized in-plane modulus – normalized area density map.

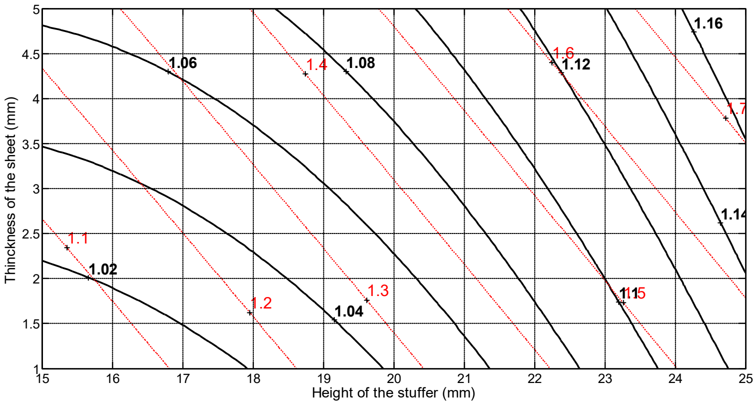

Figure 18： The normalized out-plane modulus – normalized area density map.

6 CONCLUSIONS

A mechanics-base homogenization approach is presented, resulting in two versions of the method: strain-based homogenization and stress-based homogenization. The strain-based homogenization process is obtained based on the *Principle of Virtual Displacements*; meanwhile, the stress-based homogenization process is obtained based on the *Principle of Virtual Forces*. Strain-based homogenization separates the strain field into a homogenized strain field and a strain variation field superposed on the homogenized strain field. The stress-based separates the stress field into a homogenized stress field and a stress variation field. The *Principle of Virtual Displacements* (*Principle of Virtual Forces*) for the relationship between the strain (stress) variation field and the homogenized strain (stress) field is then used to condense the strain (stress) variation field to the homogenized strain (stress) field, and the homogenization processes become coordinate reduction similar to the Guyan Reduction.

The new derivation in this paper provides improved engineering insight and enhanced physical understanding for dealing with boundary conditions, internal forces, and other issues in homogenization modeling processes. The stress-based homogenization process can be extended easily to handle discrete systems, providing a bridge between discrete and continuum systems. The mode analysis and the recovery process presented in this paper are useful tools for failure mode prediction, failure mode management, and design optimization of architectured materials.

The new method provides a way to further improve the accuracy and efficiency of multi-scale analysis problems, especially in nonlinear and structural dynamics analyses, and it more easily extended to handle various mechanical simulation and design problems. The newly derived method has been utilized to obtain effective material properties of the architectured cellular materials discussed in this paper.

REFERENCES

[1] Z.-D. Ma, Three-dimensional auxetic structures and applications thereof, *US Patent* 7,910,193 B2, 2011.

[2] Z.-D. Ma, Lightweight, rigid composite structures, *US Patent* 7,563,497 B2, 2009.

[3] E. Weinan, B. Engquist, X. Li, W. Ren, E. Vanden-Eijnden, The ~~heterogeneous~~ multiscale methods: a review. *Communications in Computational Physics*, ISSN 1815-2406, 2 (3), 367-450.

[4] P. Kanouté, D. P. Boso , J. L. Chaboche, B. A. Schrefler, Multiscale methods for composites: a review, *Archives of Computational Methods in Engineering*, 16 (1), 31-75, 2009.

[5] V. P. Nguyen, M. Stroeven, L. J. Sluys, Multiscale continuous and discontinuous modeling of heterogeneous materials: a review on recent developments, *Journal of Multiscale Modelling*, 3 (4), 1–42, 2011.

[6] E. Sanchez-Palencia Non-homogenous media and vibration theory. *Lect Notes Phys*, 127, 1980.

[7] A. Benssousan, JL, Lions, G. Papanicoulau, Asymptotic analysis for periodic structures. *Amesterdam*, North Holland, 1978.

[8] D. Cioranescu, JSJ. Paulin, Homogenization in open sets with holes. *J Math Aanal Appl,* 71, 590-607, 1979.

[9] MP Bendsùe, N. Kikuchi, Generating optimal topologies in structural design using homogenization method. *Comp Meth Appl Mech Engng*, 71, 197-224, 1988.

[10] Z.-D. Ma, N. Kikuchi, H.-C. Cheng, Topological design for vibrating structures. *Comp Meth Appl Mech Engng*, 121, 259-280, 1995.

[11] K. Matsui, K. Terada, “Continuous approximation of material distribution for topology optimi-

zation. *Int. J. Numer. Meth. Engng*, 59, 1925-1944, 2004.

[12] F. Dos Reis, J.F. Ganghoffer, Discrete homogenization of architectured materials: implementation of the method in a simulation tool for the systematic prediction of their effective elastic properties, *TECHNISCHE MECHANIK*, 30, 1 (3), 85–109, 2010.

[13] S. Arabnejad, D. Pasini, Mechanical properties of lattice materials via asymptotic homogenization and comparison with alternative homogenization methods. *International Journal of Mechanical Sciences*, 77, 249–262, 2013.

[14] K. Terada, N. Kikuchi, A class of general algorithms for multi-scale analyses of heterogeneous media, Comput. Methods Appl. Mech. Engrg. 190, 40-41, 2001.

[15] A. Abdulle, Y. Bai, Reduced-order modelling numerical homogenization. *ANMC, Mathematics Section*, École Polytechnique Fédérale de Lausanne, 1015 Lausanne, Switzerland, 2014.

[16] Y. Cong, S. Nezamabadi, H. Zahrouni, J. Yvonnet, Multiscale computational homogenization of heterogeneous shells at small strains with extensions to finite displacements and buckling. *Int. J. Numer. Meth. Engng*, 104 (4), 235-259, 2015.

[17] R.J. Guyan, Reduction of stiffness and mass matrices. *AIAA Journal*, 3 (2), 380, 1964.

[18] R. S. Lakes, Advances in negative Poisson's ratio materials. *Advanced Materials*, 5, 293-296, 1993.

APPENDIX A: GUYAN REDUCTION

Guyan Reduction [17] is well known and widely used in the analyses of finite element-based structure dynamics problems to reduce the size of the problem to be solved. It is assumed that the finite element equation of a substructure can be written as:

$$\mathbf{m}\ddot{\mathbf{u}} + \mathbf{k}\mathbf{u} = \mathbf{f} \tag{A-1}$$

where $\mathbf{u}$ stands for the nodal coordinate vector of the finite element model; $\mathbf{m}$, $\mathbf{c}$, $\mathbf{k}$, and $\mathbf{f}$ stand for the mass matrix, damping matrix, stiffness matrix, and nodal force vector of the structure, respectively.

The Guyan Reduction process divides the nodal coordinates $\mathbf{u}$ as

$$\mathbf{u} = \begin{Bmatrix} \mathbf{u}_I \\ \mathbf{u}_J \end{Bmatrix}, \tag{A-2}$$

where $\mathbf{u}_J$ contains the remaining coordinates (in which force is applied), and $\mathbf{u}_I$ contains the coordinates to be condensed (in which no force is applied). One can rewrite the corresponding static problem of Eq. (A-1) as

$$\begin{cases} \mathbf{k}_{II}\mathbf{u}_I + \mathbf{k}_{IJ}\mathbf{u}_J = \mathbf{0} \\ \mathbf{k}_{JI}\mathbf{u}_I + \mathbf{k}_{JJ}\mathbf{u}_J = \mathbf{f}_J \end{cases}. \tag{A-3}$$

Because there is no force applied on $\mathbf{u}_I$, $\mathbf{u}_I$ can be consider a function depending on $\mathbf{u}_J$; namely, we can find a matrix $\mathbf{X}$ that satisfies

$$\mathbf{u}_I = \mathbf{X}\mathbf{u}_J. \tag{A-4}$$

Substituting Eq. (A-4) into the first row equation in Eq. (A-3) gives

$$\mathbf{X} = -\mathbf{k}_{II}^{-1}\mathbf{k}_{IJ}. \tag{A-5}$$

Substituting Eqs. (A-4) and (A-5) into the second row equation in Eq. (A-3) gives

$$\mathbf{k}^{*}\mathbf{u}_J = \mathbf{f}_J, \tag{A-6}$$

where, $\mathbf{k}^{*}$ in Eq. (A-7) is called the reduced stiffness matrix (or condensed stiffness matrix, effective stiffness matrix),

$$\mathbf{k}^{*} = \mathbf{k}_{JJ} - \mathbf{k}_{JI}\mathbf{k}_{II}^{-1}\mathbf{k}_{IJ}. \tag{A-7}$$

Equations (A-4) and (A-5) can also be used to condense the mass matrix in Eq. (A-1), and we have

$$\mathbf{m}^{*} = \mathbf{m}_{JJ} + \mathbf{X}^{T}\mathbf{m}_{IJ} + \mathbf{m}_{JI}\mathbf{X} + \mathbf{X}^{T}\mathbf{m}_{II}\mathbf{X}, \tag{A-8}$$

where $\mathbf{m}^{*}$ is called the reduced mass matrix.